LETTERS

An unconventional myosin in *Drosophila* reverses the default handedness in visceral organs

Shunya Hozumi[1], Reo Maeda[1], Kiichiro Taniguchi[1], Maiko Kanai[1], Syuichi Shirakabe[1], Takeshi Sasamura[1], Pauline Spéder[3], Stéphane Noselli[3], Toshiro Aigaki[4], Ryutaro Murakami[5] & Kenji Matsuno[1,2]

The internal organs of animals often have left–right asymmetry[1,2]. Although the formation of the anterior–posterior and dorsal–ventral axes in *Drosophila* is well understood, left–right asymmetry has not been extensively studied. Here we find that the handedness of the embryonic gut and the adult gut and testes is reversed (not randomized) in viable and fertile homozygous *Myo31DF* mutants. *Myo31DF* encodes an unconventional myosin, *Drosophila* MyoIA (also referred to as MyoID in mammals; refs 3, 4), and is the first actin-based motor protein to be implicated in left–right patterning. We find that Myo31DF is required in the hindgut epithelium for normal embryonic handedness. Disruption of actin filaments in the hindgut epithelium randomizes the handedness of the embryonic gut, suggesting that Myo31DF function requires the actin cytoskeleton. Consistent with this, we find that Myo31DF colocalizes with the cytoskeleton. Overexpression of Myo61F, another myosin I (ref. 4), reverses the handedness of the embryonic gut, and its knockdown also causes a left–right patterning defect. These two unconventional myosin I proteins may have antagonistic functions in left–right patterning. We suggest that the actin cytoskeleton and myosin I proteins may be crucial for generating left–right asymmetry in invertebrates.

Mechanisms that create characteristic left–right asymmetry have been studied extensively in vertebrates[2]. However, although the organs of many invertebrate species also have left–right asymmetry, the mechanisms by which this asymmetry arises are largely unknown. In *Drosophila*, several organs have left–right asymmetry, including the embryonic gut, the adult brain and the genitalia[5–9].

To identify genes involved in left–right asymmetry of the *Drosophila* embryonic gut, we performed a genetic screen using a collection of P-element lines (Gene Search, http://gsdb.biol.metro-u.ac.jp/%7Edclust/). The embryonic gut is composed of three major parts, the foregut, midgut and hindgut, all of which have characteristic left–right asymmetry[5] (Fig. 1c, e, h and Table 1, row 1). We found that 75.7% of homozygous $Myo31DF^{souther}$ embryos show synchronous inversion of the midgut and hindgut (Fig. 1d, f and Table 1, row 2). In these embryos, the hindgut and midgut are the mirror-image of those in wild-type embryos, rather than showing randomized patterning (binominal test, $P \leq 0.01$). In contrast, foregut handedness was normal in all cases examined, indicating that this phenotype was heterotaxic (Fig. 1i and Table 1, row 2). $Myo31DF^{souther}$ is a background mutation of the Gene Search *Drosophila* line GS14508. We used deficiency mapping to map the cytological location of $Myo31DF^{souther}$ to between 30D and 31F (data not shown). We then performed complementation tests between $Myo31DF^{souther}$ and lines bearing mutations that map to this region. $Myo31DF^{souther}$ failed to complement $Myo31DF^{K1}$ (described in ref. 10), an allele of *Myo31DF* encoding *Drosophila* MyoID[3,4].

The transposable element *gypsy* was inserted into the 5′-untranslated region of the *Myo31DF* gene in $Myo31DF^{souther}$ (Fig. 1a). $Myo31DF^{L152}$ was one of five ethylmethanesulfonate (EMS)-induced *Myo31DF* alleles isolated in a large-scale EMS mutant screen (details of the screen will be presented elsewhere). $Myo31DF^{L152}$ has a base substitution that introduces a premature stop codon at amino acid 331, resulting in a putative truncated product (Fig. 1a). Myo31DF overexpression from *UAS-Myo31DF* driven by *byn–Gal4* in the hindgut and posterior midgut and their primordial counterparts rescued the left–right defects of $Myo31DF^{souther}$ embryos (Supplementary Table 1, row 22)[11], indicating that *Myo31DF* was responsible for the heterotaxia. In $Myo31DF^{souther}$ embryos, NP2432-driven expression of Myo31DF in the hindgut epithelium (Table 1, row 12), but not in other parts of the embryonic gut, such as the midgut and mesoderm (Supplementary Table 1, rows 24 and 25), was sufficient to rescue this heterotaxia, suggesting that *Myo31DF* is required in the hindgut epithelium. Furthermore, the frequency of the handedness defect was similar in $Myo31DF^{L152}$ homozygous and $Myo31DF^{L152}$/*Df(2L)J2* embryos (Table 1, rows 3 and 4; see Methods). Thus, $Myo31DF^{L152}$ is probably a null mutant of *Myo31DF*. All homozygous *Myo31DF* mutants isolated in this study were viable and fertile, with normal hindgut tissue specification, suggesting that *Myo31DF* function is largely restricted to left–right patterning (data not shown). We did not detect a maternal phenotype or *Myo31DF* gene contribution ($0.2 < P < 0.3$, χ^2 test; Supplementary Table 1, rows 5 and 6). Notably, the foregut became a mirror-image of its wild-type counterpart when *Myo31DF* was overexpressed in the entire embryo, but other parts of the gut were normal[12] (Fig. 1j and Supplementary Table 1, row 7). Therefore, we suggest that *Myo31DF* is not involved in the left–right asymmetrical development of the foregut in wild-type embryos, but can reverse foregut handedness.

We next examined the adult hindgut and testes, which are regenerated during metamorphosis. These also showed inversed handedness in the *Myo31DF* homozygote (Fig. 1l, n, p and Table 1, rows 2 and 3). In most $Myo31DF^{L152}$ adults, the loop of the hindgut and spiral of the testes were reversed (binominal test, $P \leq 0.01$), although not always synchronously (Table 1, row 3). We then knocked-down the function of the *Myo31DF* gene using RNA interference (RNAi) *in vivo*. The expression of double-stranded *Myo31DF* RNA driven by *byn–Gal4* caused inversion of the adult, but not the embryonic, hindgut (Supplementary Table 1, row 9). Thus, the left–right pattern involving *Myo31DF* is not transmitted during metamorphosis.

[1]Department of Biological Science and Technology, and [2]Genome and Drug Research Center, Tokyo University of Science, 2641 Yamazaki, Noda, Chiba 278-8510, Japan. [3]Institute of Signalling, Developmental Biology & Cancer, UMR6543-CNRS, University of Nice Sophia-Antipolis, Parc Valrose, 06108 Nice Cedex 2, France. [4]Department of Biological Science, Tokyo Metropolitan University, 1-1 Minami-osawa, Hachioji, Tokyo 192-0397, Japan. [5]Department of Physics, Biology, and Informatics, Yamaguchi University, 1677-1 Yoshida, Yamaguchi, Yamaguchi 753-8512, Japan.

In situ hybridization revealed *Myo31DF* expression in the amnioproctodeal invagination at stage 6 (Fig. 2a). At stages 12–14, *Myo31DF* messenger RNA was strongly detected in the primordial midgut and hindgut (Fig. 2b), and in the proventriculus, midgut and hindgut (Fig. 2c). A sense-strand probe of *Myo31DF* gave no detectable signal (Fig. 2d). Immunostaining of wild-type embryos with an anti-Myo31DF antibody (anti-Myo31DF-1P) also labelled the midgut and hindgut (Fig. 2e–g). These signals were absent in $Myo31DF^{souther}$ and $Myo31DF^{L152}$ homozygotes, indicating that the staining was specific (Fig. 2h and data not shown). *Myo31DF* mRNA and protein were detected in a symmetrical pattern before the development of left–right asymmetry (data not shown). Myo31DF protein is expressed in the adult gut[4]. We did not detect Myo31DF expression in the foregut, which may account for the absence of any laterality defect in the foregut of *Myo31DF* mutants.

Myo31DF protein binds to actin in an ATP-dependent manner[4]. We next examined the co-localization of Myo31DF and the actin cytoskeleton in cultured *Drosophila* S2 cells. A green fluorescent protein (GFP)-tagged Myo31DF (Myo31DF–GFP) had wild-type

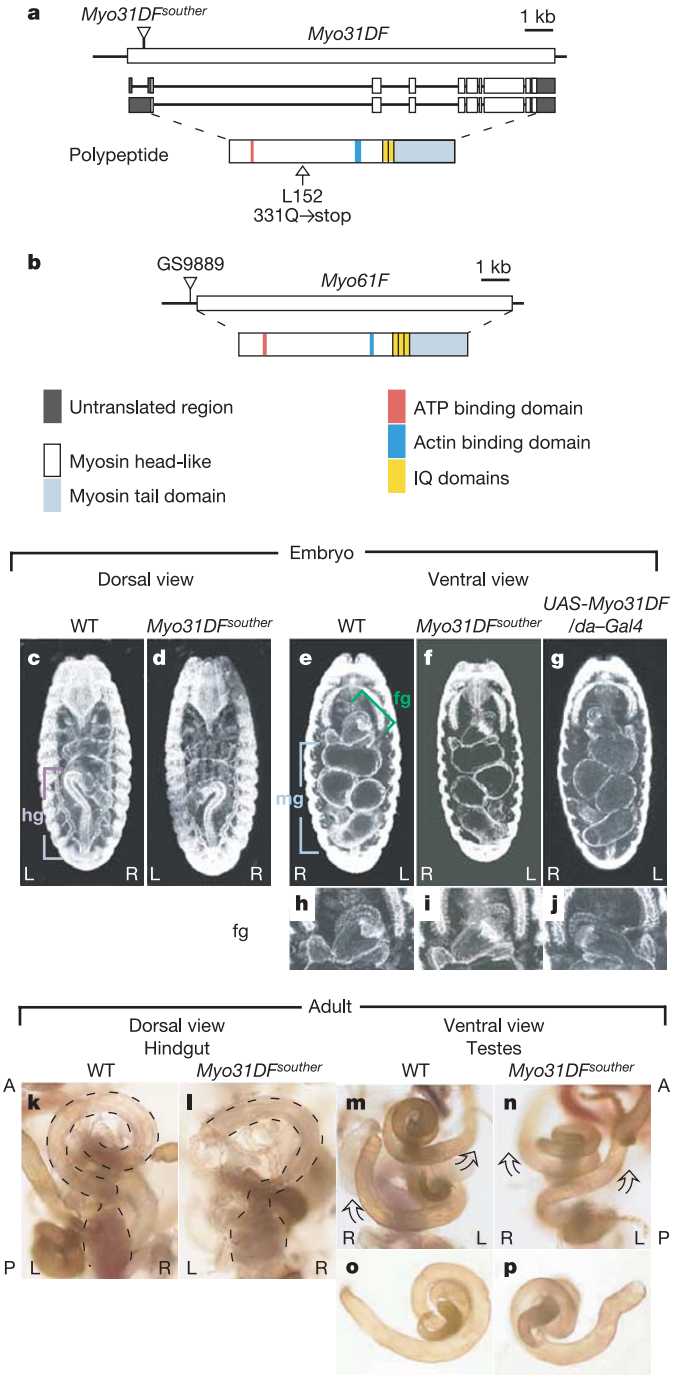

Figure 1 | *Myo31DF* mutation inverses the handedness of embryonic and adult visceral organs. **a**, Schematic of molecular lesions in $Myo31DF^{L152}$ and $Myo31DF^{souther}$. **b**, In the GS9889 line, a GS vector is inserted upstream of the *Myo61F* locus. Motifs in *Myo31DF* and *Myo61F* are shown. **c**, **e**, Wild-type embryos. **d**, **f**, $Myo31DF^{souther}$ embryos. **g**, Embryo overexpressing *Myo31DF* driven by *da–GAL4*. **h**–**j**, Higher-magnification views of the foregut images shown in **e**–**g**. **k**, Wild-type adult hindgut. **l**, $Myo31DF^{souther}$ adult hindgut. **m**, Wild-type adult with testes located anteriorly and posteriorly, elongating to the left and right, respectively. **n**, $Myo31DF^{souther}$ adult, showing mirror-image handedness of testes. **o**, **p**, Testes viewed from the ejaculatory duct in wild-type (**o**) and $Myo31DF^{souther}$ (**p**) adults. Abbreviations: fg, foregut; hg, hindgut; mg, midgut; L, left; R, right; A, anterior; P, posterior.

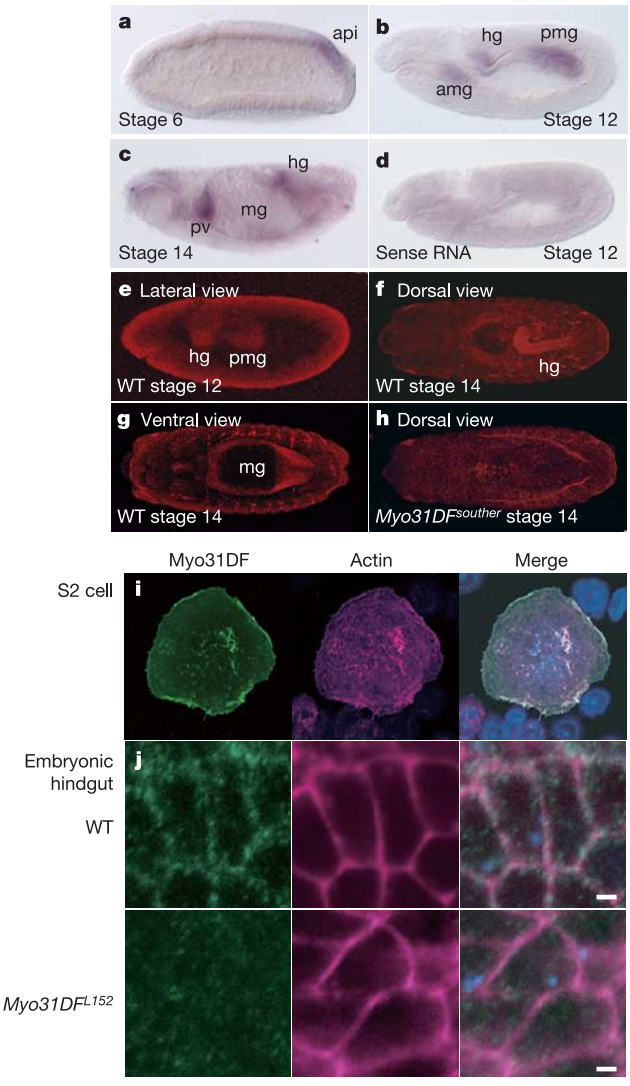

Figure 2 | Embryonic expression of *Myo31DF* and the subcellular localization of Myo31DF. **a**–**d**, *In situ* hybridization showing embryonic expression of *Myo31DF* at stage 6 (**a**), stage 12 (**b**) and stage 14 (**c**). **d**, Staining with a *Myo31DF* sense-strand RNA probe. **e**–**h**, Myo31DF detected with anti-Myo31DF-1P antibody in wild-type (WT, **e**–**g**) and $Myo31DF^{souther}$ (**h**) embryos at stage 12 (**e**) and stage 14 (**f**–**h**). **i**, **j**, Localization of Myo31DF in S2 cells (**i**) and hindgut epithelial cells (**j**). Myo31DF–GFP (**i**, left) and endogenous Myo31DF (**j**, left) are green, actin (**i**, **j**, middle) is purple; toto3 nuclear staining is blue. Right panels show the merged images. Scale bar, 1 μm. Abbreviations: amg, anterior midgut primordium; api, amnioproctodeal invagination; hg, hindgut; mg, midgut; pmg, posterior midgut primordium; pv, proventriculus.

Table 1 | Percentage of flies showing handedness defects

Genotype	Embryonic phenotype					Adult phenotype			
	Foregut inverse	Foregut deformed	Midgut inverse	Hindgut inverse	Midgut and hindgut deformed	Hindgut inverse	Hindgut deformed	Testis inverse	Testis deformed
Wild-type	0.5(1/200)	2.5(5/200)	0.4(1/247)	0.4(1/247)	2.4(7/247)	0.0(0/55)	0.0(0/55)	0.0(0/56)	7.1(4/56)
Myo31DF^{souther}	0.0(0/51)	0.0(0/51)	75.7(28/37)	75.7(28/37)	5.4(2/37)	40.7(22/54)	29.6(16/54)	73.7(28/38)	18.4(7/38)
Myo31DF^{L1S2}	1.9(1/51)	0.0(0/51)	82.0(105/128)	82.0(105/128)	6.3(8/128)	85.7(30/35)	2.9(1/35)	78.7(37/47)	19.1(9/47)
Myo31DF^{L1S2} / Df(2L)J2	-	-	57.7(30/52)	61.5(31/52)	6.0(3/52)	-	-	-	-
UAS-gfp-moesin / byn-Gal4	0.0(0/41)	0.0(0/41)	29.4(5/17)	47.5(28/59)	0.0(0/59)	-	-	-	-
Myo31DF^{L1S2}; UAS-gfp-moesin / byn-Gal4	0.0(0/8)	0.0(0/8)	60.0(3/5)	52.8(19/36)	0.0(0/36)	-	-	-	-
UAS-Rho N19 / NP2432	-	-	28.9(22/76)	21.0(16/76)	9.2(7/76)	-	-	-	-
UAS-Myo61F / byn-Gal4	-	-	100.0(17/17)	100.0(36/36)	0.0(0/36)	-	-	-	-
UAS-Myo31DF / byn-Gal4	-	-	0.0(0/47)	0.0(0/47)	0.0(0/47)	-	-	-	-
UAS-dsRNA Myo61F / P{Gal4-nos.NGT}40	1.5(1/65)	0.0(0/65)	7.7(5/65)*	0.0(0/65)	1.5(1/65)	-	-	-	-
Rescue experiments (*Myo31DF^{souther}* background)									
UAS-Myo31DF /+	-	-	46.3(37/80)	46.3(37/80)	2.5(2/80)	-	-	-	-
UAS-Myo31DF / NP2432	-	-	0.0(0/40)	0.0(0/40)	7.5(3/40)	-	-	-	-

The percentage of embryos showing defects in handedness (inverse) or deformation of organs (deformed) is shown. Genotypes of the examined embryos and adults are indicated on the left. Actual numbers of scored embryos and adults are shown in parentheses.
-, values not determined.
*Embryos showing partial inversion of midgut handedness are included.

function, given that its overexpression rescued *Myo31DF^{souther}* (Supplementary Table 1, row 26). Myo31DF–GFP co-localized with actin, mostly at cell protrusions (Fig. 2i). In epithelial cells of the hindgut, endogenous Myo31DF was detected as punctate staining, partly overlapping with cortical actin (Fig. 2j).

byn–Gal4-driven misexpression of GFP-tagged moesin, an actin-binding protein, in wild-type embryos caused a reduction in actin filaments in the apical region of the hindgut epithelium, where Myo31DF function is required[13] (Fig. 3a,b). Notably, the midgut and hindgut always had the same handedness, but the handedness was random (not inversed), in wild-type and *Myo31DF* homozygous embryos (Table 1, rows 5 and 6). Embryo handedness was also affected by NP2432-driven GFP–moesin expressed in the hindgut epithelium only (Supplementary Table 1, row 12). However, GFP–moesin expression in the midgut only did not affect handedness (Supplementary Table 1, row 13).

To investigate further the functional link between Myo31DF and the actin cytoskeleton, we determined the phenocritical period for inducing left–right defects using *Myo31DF* RNAi and GFP–moesin misexpression, following the TARGET method[14]. Both *Myo31DF* knockdown and GFP–moesin expression in the hindgut 0–24 h after pupation caused similar defects in adult gut handedness, suggesting that Myo31DF and the appropriate organization of actin filaments are required at the same time (Supplementary Table 2). GFP–moesin also affected handedness in the *Myo31DF* embryo, suggesting that the default handedness, which may be manifested in the *Myo31DF* homozygote, also depends on the actin cytoskeleton (Table 1, row 6). We also examined the involvement of three Rho GTPase family proteins, Rho, Rac and Cdc42, which regulate the organization of the actin cytoskeleton[15]. Expression of dominant-negative forms of these proteins, especially Rho, in the hindgut induced synchronous left–right defects in the embryonic midgut and hindgut (Table 1, row 7 and Supplementary Table 1, rows 14 and 16). Together, our results suggest that *Myo31DF* depends on the actin cytoskeleton to generate left–right asymmetry.

Cell division and cell death do not occur during left–right asymmetric development of the hindgut[16]. We therefore speculated that the rearrangement of hindgut epithelial cells may be part of this

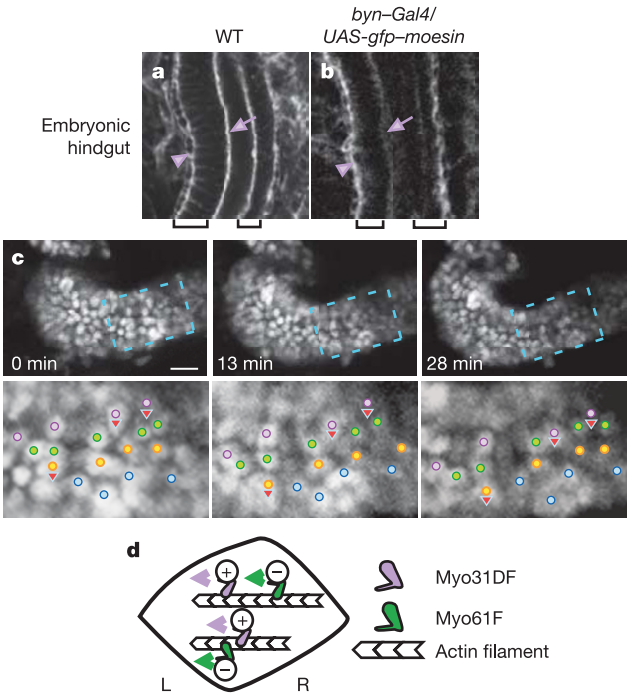

Figure 3 | Myo31DF is dependent on the actin cytoskeleton to develop left–right asymmetry. a, **b**, Actin localization in hindgut epithelium of wild-type (**a**) and GFP–moesin-overexpressing (**b**) embryos. The basal surface is indicated with an arrowhead, the apical surface with an arrow, and hindgut epithelial cell layers are indicated with brackets. **c**, Time-lapse analysis of hindgut epithelial cells. Dots of each colour indicate a single row of cells at $t = 0$ min. Images obtained at 0, 13 and 28 min are shown. The lower panels show a higher magnification image of the boxed area in each upper panel. Note that each row of cells tilts (with right becoming upper), which coincides with the left-handed rotation of the hindgut. Cells showing intercalation are indicated with arrowheads showing the direction of their movement. Scale bar, 10 μm. **d**, Model for myosin I protein functions in *Drosophila* left–right asymmetry. Myo31DF and Myo61F transport left–right determinants with opposite activities.

process. To test this possibility, we performed a time-lapse analysis. The position of each cell was visualized by labelling the nucleus with GFP. Cell rearrangement, which coincided with the left–right bias associated with left-handed rotation of the hindgut, was suggested by the significant intercalation of some cells (arrowheads in Fig. 3c).

Another myosin I protein, Myo61F (*Drosophila* MyoIB, also referred to as MyoIC in mammals), has been reported in *Drosophila*[3,4,17]. Myo61F protein is detected in the embryo and adult gut[4]. To test whether *Myo61F* is also involved in left–right asymmetry, we overexpressed *Myo61F* using *UAS-Myo61F* or GS9889 driven by *byn–Gal4* (Gene Search; Fig. 1b). Unexpectedly, Myo61F overexpression resulted in inversion of the midgut and hindgut in both cases (Table 1, row 8, and data not shown). In contrast, *Myo31DF* overexpression did not affect the handedness of these organs (Table 1, row 9). These results suggest that Myo31DF and Myo61F have antagonistic functions in creating the left–right asymmetry of these organs. The involvement of Myo61F in left–right asymmetry is also supported by our finding that its knockdown by RNAi results in the left–right defect in the embryonic midgut (Table 1, row 10).

We have found that homozygous *Myo31DF* embryos show reversed handedness of embryonic and adult visceral organs, which may represent the default state of left–right asymmetry in *Drosophila*. This situation is similar to the function of the *sinistral* gene in the freshwater snail, *Limnea* (although the *sinistral* gene is required maternally)[1,18]. Normal handedness is still seen in 25% of *Myo31DF* homozygotes. We speculate that some other myosin gene(s) has a redundant function in left–right patterning. Inversion of the anteroposterior axis does not affect laterality, suggesting that left–right pattering occurs zygotically[7]; this is consistent with the zygotic function of *Myo31DF*. Our results also suggest that an actin-based mechanism, which can align itself to either an anteroposterior–dorsoventral reference or the pre-existing sinistral handedness, exists to direct the rotation of the hindgut epithelium. As myosin I proteins are involved in vesicular transport[19], we propose that Myo31DF and Myo61F, which on the basis of their structures are believed to move to the plus ends of actin filaments, carry left–right determinants with opposite activities (Fig. 3d). Thus, both left–right determinants would be concentrated in the plus ends of actin filaments that have a hypothetical planar polarity. In the *Myo31DF* mutant, only the opposing determinant is concentrated here, which reverses the handedness. According to our model, disruption in actin organization would result in left–right randomization, as we indeed observed experimentally.

METHODS

***Drosophila* stocks.** We used Canton-S as the wild-type *Drosophila* strain. $Myo31DF^{souther}$ and $Myo31DF^{L152}$ are newly characterized *Myo31DF* mutations. GS9889 is a Gene Search line. *Df(2L)J2* has a deletion between 31B and 32A (Bloomington Stock Center). The following GAL4 drivers were used: *byn–Gal4* drives GAL4 expression in the hindgut and the posterior midgut primordium at stage 8, and in the longitudinal visceral mesoderm at stage 11 (ref. 11). *da–Gal4* drives uniform GAL4 expression[12]. how^{24B} drives GAL4 expression in the mesoderm primordium from stage 11 (ref. 20). 48Y drives GAL4 expression in the anterior and posterior midgut primordium from stage 10 (ref. 21). NP2432 drives GAL4 expression in the hindgut epithelium from stage 9 (fly stock from National Institute of Genetics, http://www.shigen.nig.ac.jp/fly/nigfly; data not shown). NP5021 drives GAL4 expression in the whole gut from stage 9 (fly stock from National Institute of Genetics; data not shown). *P{Gal4–nos.NGT}40* expresses *Gal4* mRNA maternally[22].

The following *UAS* lines were used: *UAS-gfp–moesin*, which encodes a fusion protein of the actin-binding domain of moesin and GFP (provided by S. Hayashi)[13]; *UAS-Rho N19* (ref. 23); *UAS-Rac1 N17* (ref. 24); *UAS-Cdc42 F89* (ref. 25); *UAS-Myo31DF* (provided by S. Noselli); *UAS-Myo31DF–GFP* and *UAS-2* × $Myo31DF^{RNAi}$. The last two UAS lines are described in the accompanying paper[10].

UAS-Myo61F lines carry a pUAST transformation vector that has an insertion of the entire open reading frame of *Myo61F* cDNA (clone GH04201). *UAS*-dsRNA *Myo61F* lines carry a construct in which *Myo61F* cDNA corresponding to nucleotides 446–848 of GH04201 was inserted into pUAST as an inverted repeat with an interruption of the *Myo61F* fourth intron. *UAS*-dsRNA *Myo61F* was maternally driven by *P{Gal4–nos.NGT}40*. The genotypes of each embryo were determined using appropriate blue-balancers, such as *CyO, P{en1}*wg^{en11} and *TM3, ftz-lacZ*. All crosses, except those used for the TARGET analysis, were performed at 25 °C on standard *Drosophila* medium.

Analysis of phenocritical periods. We used the TARGET method to determine the phenocritical periods for inducing the left–right defect of the adult gut by knocking down *Myo31DF* and expressing of GFP–moesin[14]. We used a temperature-sensitive GAL80, a suppressor of GAL4, to control the activity of GAL4 driven by *byn–Gal4*. This allowed us to express a double-stranded RNA corresponding to a portion of *Myo31DF* mRNA and to express GFP–moesin in a temporally specific manner. Flies were cultured at 18 °C, and pupae were collected at 24-h intervals. Pupae collected 0–24, 24–48 and 48–72 hours after pupation were cultured at 30 °C until eclosion.

Histological analyses of embryos. Antibody staining of *Drosophila* embryos was performed as previously described[26]. Embryos were photographed using Zeiss Axioskop2 plus or Zeiss Pascal microscopes. Primary antibodies were a mouse anti-Fasciclin III antibody (7G10, Developmental Studies Hybridoma Bank; 1:100 dilution)[27] and a rabbit anti-Myo31DF-1P antibody (1:10 dilution). The anti-Myo31DF-1P rabbit serum was raised against a glutathione *S*-transferase fusion protein containing Myo31DF amino acids 728–990 (also described in ref. 10). The anti-Myo31DF-1P antibody was affinity purified using the same Myo31DF polypeptide with a His-tag. Secondary antibodies were Cy3 anti-rabbit IgG, Cy3 anti-mouse IgG, and anti-rabbit Alexa488 (Jackson ImmunoResearch; used at 1:1,000 dilution). Toto3 was used as a nuclear marker (Molecular Probes; 1:200 dilution). Actin filaments were stained with rhodamine–phalloidin[28] (Molecular Probes; 1:200 dilution). Whole-mount *in situ* hybridization was carried out as described[29]. A digoxigenin-labelled RNA probe was prepared from a full-length cDNA template of *Myo31DF* using a DIG RNA labelling kit (Roche).

Microscopic analysis of embryonic gut handedness. Genotypes of the embryos that were selected for study were identified by the lack of blue-balancers after β-galactosidase staining[26]. The handedness of the foregut, midgut and hindgut were scored at stages 15–16, stage 16, and stages 14–16, respectively.

Cell culture and staining. *Drosophila* S2 cells were plated and cultured on concanavalin A (Sigma) as previously described[30]. The cells were co-transfected with pUAS-*Myo31DF–GFP* and pAyGAL4 using CellFECTIN (Invitrogen). S2 cells were fixed and stained as described[30]. The secondary antibody used was anti-rabbit Alexa488 (Jackson ImmunoResearch; 1:200 dilution). Staining with rhodamine–phalloidin (1:40 dilution) was carried out as described[28]. The nuclear marker was toto3 (1:200 dilution).

Time-lapse analysis. Live embryos expressing NP5021-driven $UAS\text{-}GFP^{nls}$ in the whole gut were mounted with FL-100 (Shin-Etsu Chemical Co.). Images were collected on a Zeiss Pascal microscope at intervals of 25 s from stage 13 onwards, and were processed with Zeiss LSM Image Browser and Adobe Photoshop software.

Received 20 September 2005; accepted 2 February 2006.

1. Wood, W. B. Left–right asymmetry in animal development. *Annu. Rev. Cell Dev. Biol.* **13,** 53–82 (1997).
2. Mercola, M. & Levin, M. Left–right asymmetry determination in vertebrates. *Annu. Rev. Cell Dev. Biol.* **17,** 779–805 (2001).
3. Gillespie, P. G. *et al.* Myosin-I nomenclature. *J. Cell Biol.* **155,** 703–704 (2001).
4. Morgan, N. S., Heintzelman, M. B. & Mooseker, M. S. Characterization of Myosin-IA and Myosin-IB, two unconventional myosins associated with the *Drosophila* brush border cytoskeleton. *Dev. Biol.* **172,** 51–71 (1995).
5. Hayashi, T. & Murakami, R. Left–right asymmetry in *Drosophila melanogaster* gut development. *Dev. Growth Differ.* **43,** 239–246 (2001).
6. Ligoxygakis, P., Strigini, M. & Averof, M. Specification of left–right asymmetry in the embryonic gut of *Drosophila*. *Development* **128,** 1171–1174 (2001).
7. Hayashi, M. *et al.* Left–right asymmetry in the alimentary canal of the *Drosophila* embryo. *Dev. Growth Differ.* **47,** 457–460 (2005).
8. Pascual, A., Huang, K, Neven, J. & Préat, T. Neuroanatomy: Brain asymmetry and long-term memory. *Nature* **427,** 605–606 (2004).
9. Adam, G., Perrimon, N. & Noselli, S. The retinoic-like juvenile hormone controls the looping of left–right asymmetric organs in *Drosophila*. *Development* **130,** 2397–2406 (2003).
10. Spéder, P., Ádám, G. & Noselli, S. Type ID unconventional myosin controls left–right asymmetry in *Drosophila*. *Nature* doi:10.1038/nature04623 (this issue).
11. Iwaki, D. D. & Lengyel, J. A. A Delta–Notch signaling border regulated by Engrailed/Inverted repression specifies boundary cells in the *Drosophila* hindgut. *Mech. Dev.* **114,** 71–84 (2002).
12. Wodarz, A., Hinz, U., Engelbert, M. & Knust, E. Expression of crumbs confers apical character on plasma membrane domains of ectodermal epithelia of *Drosophila*. *Cell* **82,** 67–76 (1995).

13. Edwards, K. A., Demsky, M., Montague, R. A., Weymouth, N. & Kiehart, D. P. GFP–moesin illuminates actin cytoskeleton dynamics in living tissue and demonstrates cell shape change during morphogenesis in *Drosophila*. *Dev. Biol.* **191,** 103–117 (1997).
14. McGuire, S. E. *et al.* Spatiotemporal rescue of memory dysfunction in *Drosophila*. *Science* **302,** 1765–1768 (2003).
15. Etienne-Manneville, S. & Hall, A. Rho GTPases in cell biology. *Nature* **420,** 629–635 (2002).
16. Iwaki, D. D., Johansen, K. A., Singer, J. B. & Lengyel, J. A. *drumstick*, *bowl*, and *lines* are required for patterning and cell rearrangement in the *Drosophila* embryonic hindgut. *Dev. Biol.* **240,** 611–626 (2001).
17. Gillespie, P. G., Wagner, M. C. & Hudspeth, A. J. Identification of a 120 kd hair-bundle myosin located near stereociliary tips. *Neuron* **11,** 581–594 (1993).
18. Shibazaki, Y., Shimizu, M. & Kuroda, R. Body handedness is directed by genetically determined cytoskeletal dynamics in the early embryo. *Curr. Biol.* **14,** 1462–1467 (2004).
19. Huber, L. A. *et al.* Both calmodulin and unconventional myosin Myr4 regulate membrane trafficking along the recycling pathway of MDCK cells. *Traffic* **1,** 494–503 (2000).
20. Brand, A. H. & Perrimon, N. Targeted gene expression as a means of altering cell fates and generating dominant phenotypes. *Development* **118,** 401–415 (1993).
21. Martin-Bermudo, M. D., Dunin-Borkowski, O. M. & Brown, N. B. Specificity of PS integrin function during embryogenesis resides in the α subunit extracellular domain. *EMBO J.* **16,** 4184–4193 (1997).
22. Tracey, W. D. Jr, Ning, X., Klingler, M., Kramer, S. G. & Gergen, J. P. Quantitative analysis of gene function in the *Drosophila* embryo. *Genetics* **154,** 273–284 (2000).
23. Strutt, D. I., Weber, U. & Mlodzik, M. The role of RhoA in tissue polarity and Frizzled signaling. *Nature* **387,** 292–295 (1997).
24. Luo, L., Liao, Y. J., Jan, L. Y. & Jan, Y. N. Distinct morphogenetic functions of similar small GTPases: *Drosophila* Drac1 is involved in axonal outgrowth and myoblast fusion. *Genes Dev.* **8,** 1787–1802 (1994).
25. Eaton, S., Auvinen, P., Luo, L., Jan, Y. N. & Simons, K. CDC42 and Rac1 control different actin-dependent processes in the *Drosophila* wing epithelium. *J. Cell Biol.* **131,** 151–164 (1995).
26. Sullivan, W., Ashburner, M. & Hawley, R. S. Drosophila *Protocols* (Cold Spring Harbor Laboratory Press, New York, 2000).
27. Patel, N. H., Snow, P. M. & Goodman, C. S. Characterization and cloning of fasciclin III: a glycoprotein expressed on a subset of neurons and axon pathways in *Drosophila*. *Cell* **48,** 975–988 (1987).
28. Frydman, H. M. & Spradling, A. C. The receptor-like tyrosine phosphatase Lar is required for epithelial planar polarity and for axis determination within *Drosophila* ovarian follicles. *Development* **128,** 3209–3220 (2001).
29. Jiang, J., Kosman, D., Ip, Y. T. & Levine, M. The dorsal morphogen gradient regulates the mesoderm determinant twist in early *Drosophila* embryos. *Genes Dev.* **5,** 1881–1891 (1991).
30. Rogers, S. L., Rogers, G. C., Sharp, D. J. & Vale, R. D. *Drosophila* EB1 is important for proper assembly, dynamics, and positioning of the mitotic spindle. *J. Cell Biol.* **158,** 873–884 (2002).

Supplementary Information is linked to the online version of the paper at www.nature.com/nature.

Acknowledgements We thank the Developmental Studies Hybridoma Bank at the University of Iowa, the Bloomington Stock Center, and the *Drosophila* Genetic Resource Center at the Kyoto Institute of Technology. We thank J. Lengyel for *byn-Gal4* and S. Hayashi for *UAS-gfp-moesin* transgenic strains. This work was supported by grants-in-aid from the Japanese Ministry of Education, Culture, Sports and Science.

Author Contributions Experimental work was performed by S.H., R.M., K.T., M.K., S.S., T.S., P.S. and T.A. Data analysis was by S.H., R.M., K.T. and K.M., and project planning was coordinated by S.N., R.M. and K.M.

Author Information Reprints and permissions information is available at npg.nature.com/reprintsandpermissions. The authors declare no competing financial interests. Correspondence and requests for materials should be addressed to K.M. (matsuno@rs.noda.tus.ac.jp).

20. L. A. Anderson, J. L. Sarmiento, *Global Biogeochem. Cycles* **8**, 65 (1994).
21. L. A. Codispoti *et al.*, *Sci. Mar.* **65** (suppl. 2), 85 (2001).
22. C. Deutsch, N. Gruber, R. M. Key, J. L. Sarmiento, A. Ganachaud, *Global Biogeochem. Cycles* **15**, 483 (2001).
23. C. G. Castro, F. P. Chavez, C. A. Collins, *Global Biogeochem. Cycles* **15**, 819 (2001).
24. A. van Geen *et al.*, *Paleoceanography* **18**, 1098 (2003).
25. R. S. Ganeshram, T. F. Pedersen, S. E. Calvert, J. W. Murray, *Nature* **376**, 755 (1995).
26. M. A. Altabet, R. Francois, D. W. Murray, W. L. Prell, *Nature* **373**, 506 (1995).
27. H. Garcia, R. A. Locarnini, T. P. Boyer, J. I. Antonov, in *NOAA Atlas NESDros. Inf. Serv.* (U.S. Government Printing Office, Washington, DC, 2006), vol. 63.

Acknowledgments: Supported by a grant from the Gordon and Betty Moore Foundation (C.D.) and NSF grants OCE-0851483 (C.D.) and OCE-0851497 (T.I.).

Supporting Online Material
www.sciencemag.org/cgi/content/full/science.1202422/DC1
Materials and Methods
Figs. S1 to S7
References

3 January 2011; accepted 27 May 2011
Published online 9 June 2011;
10.1126/science.1202422

Chirality in Planar Cell Shape Contributes to Left-Right Asymmetric Epithelial Morphogenesis

Kiichiro Taniguchi,[1]* Reo Maeda,[1]* Tadashi Ando,[1] Takashi Okumura,[1] Naotaka Nakazawa,[1] Ryo Hatori,[1] Mitsutoshi Nakamura,[1] Shunya Hozumi,[1] Hiroo Fujiwara,[1] Kenji Matsuno[1,2]†

Some organs in animals display left-right (LR) asymmetry. To better understand LR asymmetric morphogenesis in *Drosophila*, we studied LR directional rotation of the hindgut epithelial tube. Hindgut epithelial cells adopt a LR asymmetric (chiral) cell shape within their plane, and we refer to this cell behavior as planar cell-shape chirality (PCC). *Drosophila* E-cadherin (*D*E-Cad) is distributed to cell boundaries with LR asymmetry, which is responsible for the PCC formation. Myosin ID switches the LR polarity found in PCC and in *D*E-Cad distribution, which coincides with the direction of rotation. An in silico simulation showed that PCC is sufficient to induce the directional rotation of this tissue. Thus, the intrinsic chirality of epithelial cells in vivo is an underlying mechanism for LR asymmetric tissue morphogenesis.

Directional left-right (LR) asymmetry is widely found in animals, such as in the position and structure of the heart, spleen, gut, and lung in vertebrates (*1*). The mechanisms of LR axis formation are well understood in some vertebrates (*1*), and the cellular basis for LR symmetry breaking, including cell polarities, is beginning to be elucidated (*2*, *3*). *Drosophila* shows a directional LR asymmetry of certain organs, including the embryonic hindgut (*4*, *5*). Although some unique features of *Drosophila* laterality development have been revealed, such as the involvement of myosin ID (MyoID) (*4*, *5*), the detailed mechanisms of its LR asymmetric development remain largely unknown.

The *Drosophila* embryonic hindgut begins as a symmetric midline structure that curves ventrally at stage 12 (Fig. 1A and fig. S1A). It subsequently makes a 90° left-handed rotation, forming a rightward curving structure by stage 13 (Fig. 1A) (*6*). The hindgut epithelium, but not the overlying visceral muscles, is responsible for this rotation, which is not accompanied by cell proliferation or cell death (*6*). Therefore, we speculated that the hindgut epithelial cells themselves might have LR polarity, which could contribute to the rotation.

To analyze LR polarity in the hindgut epithelial cells, we examined the locations of the centrosomes, which reflect cell polarity in other systems (*7*, *8*). We calculated each cell's centroid with respect to its boundaries and plotted the relative position of the centrosome, labeled with green fluorescent protein (GFP)–centrosomin (Fig. 1, B and C). In wild-type animals, the relative position of the centrosome was significantly biased to the right-posterior region (Fig. 1, D and E). These results suggest that hindgut epithelial cells adopt a LR polarity within their plane before the hindgut rotates.

We speculated that this LR polarity would be reflected in the cell shape and participate directly in the left-handed rotation. To address this, we measured the angle between apical cell boundaries and the antero-posterior (AP) axis of the hindgut epithelial tube before rotation (late-stage 12) (x° in Fig. 2A). These apical cell boundaries corresponds to the zonula adherens (ZA). Cell-boundary angles of −90° to 0° to the AP axis were more frequent than those of 0° to 90°, indicating that hindgut epithelial cells have a LR-biased planar cell shape (Fig. 2B). We designated this LR bias as planar cell-shape chirality (PCC), because the mirror image of the cell's planar shape does not overlap with its original cell shape.

We previously demonstrated that the hindgut rotates right-handedly in embryos homozygous for *Myo31DF*, which encodes MyoID (*4*). In *Myo31DF*^{L152} homozygotes, the distribution of angle x° was reversed from that of wild type, although the LR bias became less prominent (compare Fig. 2, B and C). The reversed PCC in *Myo31DF*^{L152} was rescued by the overexpression of *Myo31DF*^{GFP} (Fig. 2D). Rho family guanosine triphosphatases, including Rho1 and Rac1, regulate the organization of the actin cytoskeleton

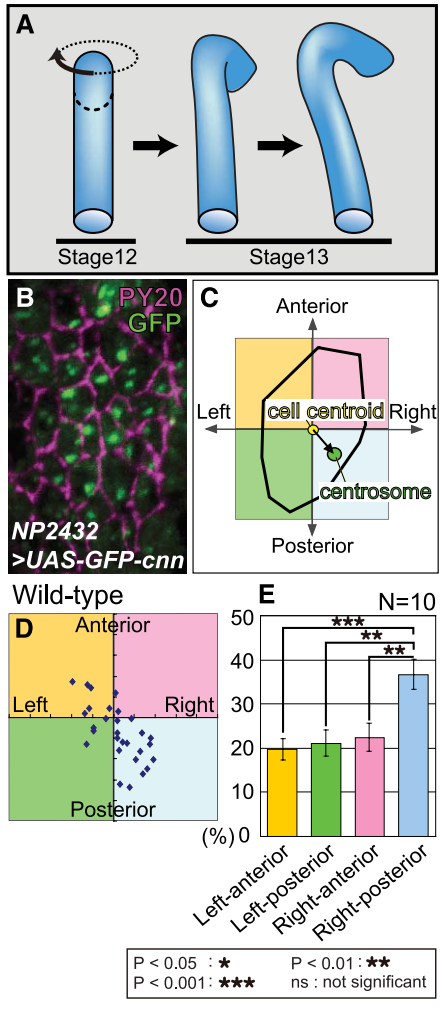

Fig. 1. Polarization of centrosome positions in hindgut epithelial cells. (**A**) Schematic drawing of the left-handed rotation of the wild-type hindgut. (**B**) Centrosomes (green) visualized by *UASp-GFP-cnn* expression driven by *NP2432*. Cell boundaries were detected by antibody against PY20 (anti-PY20) (magenta). (**C**) Diagram representing the position of a centrosome relative to the cell centroid in two-dimensional coordinates (anterior-posterior and left-right). (**D**) Representative result showing the positions of centrosomes (blue dots) in a wild-type hindgut. (**E**) Percentages of centrosomes plotted on the four areas of (D). Bars show standard errors among the means of 10 embryos.

[1]Department of Biological Science and Technology, Tokyo University of Science, 2641 Yamazaki, Noda, Chiba 278-8510, Japan. [2]Research Institute for Science and Technology, Tokyo University of Science, 2641 Yamazaki, Noda, Chiba 278-8510, Japan.

*These authors contributed equally to this work.
†To whom correspondence should be addressed. E-mail: matsuno@rs.noda.tus.ac.jp

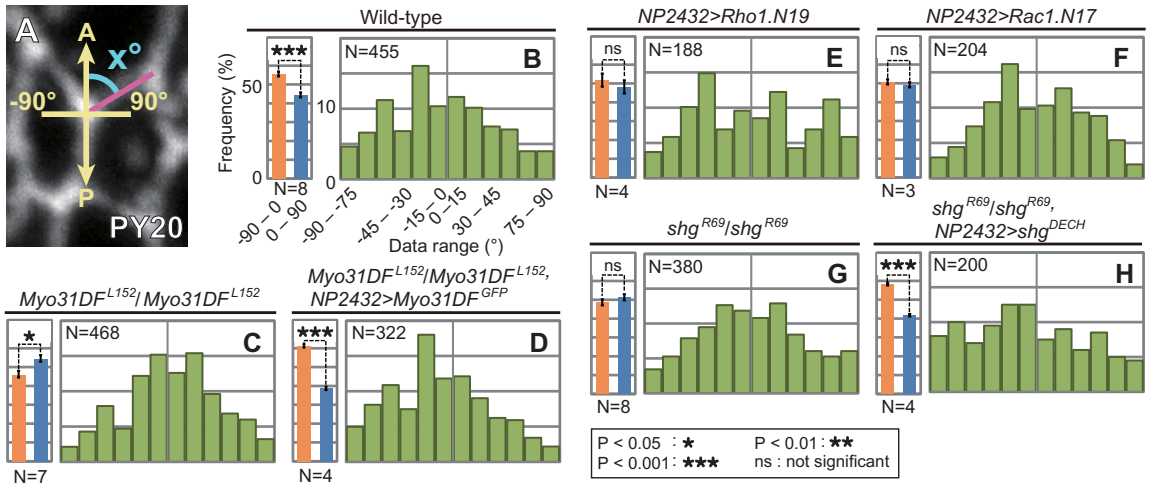

Fig. 2. Requirement for MyoID and *D*E-Cad to form normal PCC in hindgut epithelial cells. (**A**) The angle between a cell boundary (magenta) labeled with anti-PY20 and the AP axis (yellow arrow) is defined as *x*° (turquoise arc). Images of cell boundaries at the dorsal apical surface of the hindgut epithelial tube were used for analysis. (**B** to **H**) Percentage of cell boundaries with angle *x*° in the ranges indicated at the bottom of (B). Genotypes of the analyzed embryos are indicated at top. At left, graphs show the means obtained from the number of embryos indicated (N), and error bars indicate standard errors among the means. At right, graphs show the percentage of cell boundaries (N) with angle *x*° at 15° intervals.

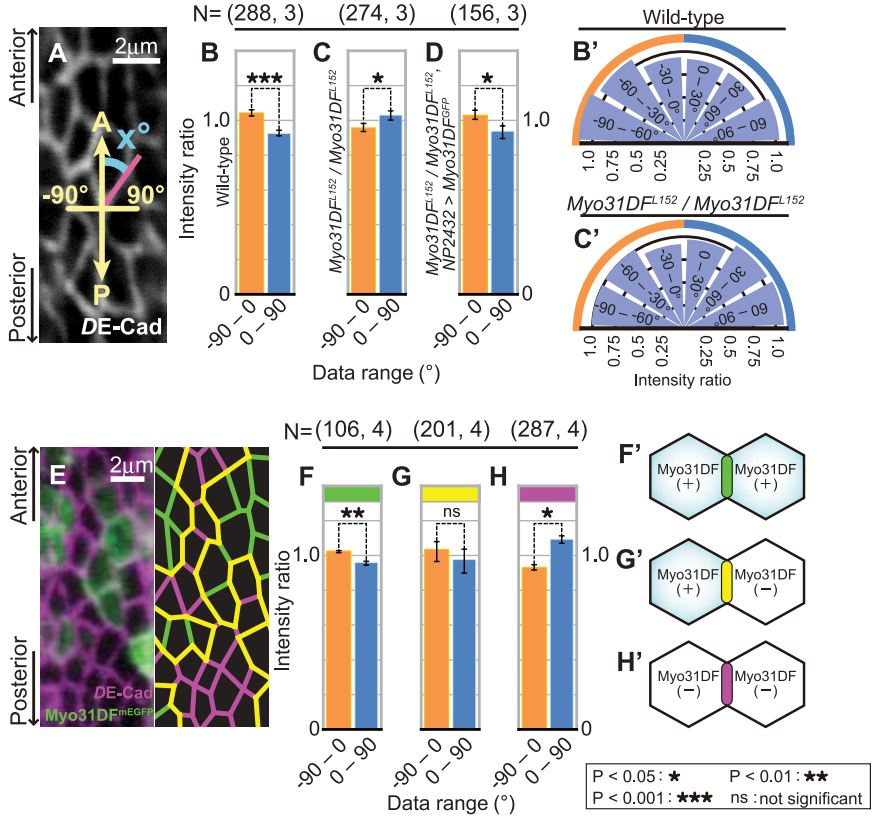

Fig. 3. Polarized distribution of *D*E-Cad. (**A**) Hindgut epithelium stained with an antibody against *D*E-Cad (anti-*D*E-Cad). See Fig. 2A for angle *x*°. (**B** to **D**) Bar graphs showing the mean of the normalized *D*E-Cad fluorescent intensities at the cell boundary in the hindgut epithelium of the indicated genotypes representing the indicated ranges of angle *x*°. (**B′** and **C′**) Rose diagrams showing the mean of normalized *D*E-Cad intensity in the hindgut epithelium of wild-type and *Myo31DF*^{L152} homozygous embryos at 30° intervals of angle *x*°. (**E**) Mosaic hindgut epithelium including *Myo31DF*^{mEGFP}-expressing (+, green) and nonexpressing cells (–) in a *Myo31DF*^{L152} homozygote. Cell boundaries composed of +/+, +/–, and –/– cells are indicated in green, yellow, and magenta, respectively (right). (**F** to **H**) Bar graphs showing the mean of normalized *D*E-Cad intensities in +/+ (F), +/– (G), and –/– (H) cell boundaries. (F′ to H′) Schematic representation of cell boundaries composed of +/+ (green), +/– (yellow), and –/– (magenta) cells. *Myo31DF*^{mEGFP}-expressing cells are shown in light blue. The number of cell boundaries and embryos analyzed are indicated as N = ($N^{cell\ boundary}$, N^{embryo}) in (B) to (D) and (F) to (H).

(*9*). We previously showed that overexpression of a dominant-negative *Rho1* (*Rho1.N19*) or *Rac1* (*Rac1.N17*) in the hindgut epithelium disrupts the hindgut's LR asymmetry (*9*). We observed no PCC in these epithelial cells, suggesting that PCC formation depends on the actin cytoskeleton (Fig. 2, E and F). These results support our suggestion that PCC could determine the subsequent laterality of the hindgut.

To identify genes involved in PCC formation, we screened for mutations affecting LR asymmetry of the hindgut. We found that *shotgun* (*shg*) mutations (*shg*^{R758}, *shg*^{R1232}, and *shg*^{R69}, a null allele) disrupted the laterality of the hindgut (fig. S1). *shg* encodes *D*E-Cad, a conserved transmembrane protein that mediates cell-cell adhesion in the epithelium (*10*). Genetic analyses suggested that *D*E-Cad functions downstream of MyoID, and both are required in the hindgut epithelium just before its rotation for normal LR asymmetric development (figs. S1D and S2). In *shg*^{R69} homozygotes, the angle *x*° did not demonstrate LR asymmetry, indicating that PCC was not formed in this mutant (compare Fig. 2, B and G). This PCC defect in *shg*^{R69} homozygotes was rescued by the overexpression of *shg*^{DECH} (Fig. 2H).

To understand how *D*E-Cad contributes to PCC formation, we examined whether the distribution of *D*E-Cad showed LR polarity in hindgut epithelial cells. For this, we calculated the mean of *D*E-Cad's relative intensity at the ZA of each cell boundary in the hindgut epithelium at late-stage 12. In wild type, the mean intensity was significantly greater at the cell boundaries with an angle *x*° of −90° to 0° than in those with 0 to 90° angles (Fig. 3, A and B), whereas this situation was reversed in *Myo31DF*^{L152} homozygotes (Fig. 3C). Rose diagrams depicting the intensity of *D*E-Cad in the cell boundaries bundled for 30° intervals showed that *D*E-Cad was enriched in cell boundaries with an angle *x*° of −90° to −30° (Fig. 3B′). Conversely, in *Myo31DF*^{L152} homozygotes, this situation was reversed (Fig. 3C′). This reversed bias was restored to the wild-type situation by overexpressing *Myo31DF*^{GFP} in the hindgut epithelium (Fig. 3D).

We then asked whether the LR bias of *D*E-Cad distribution was attributable to a cell-autonomous function of MyoID. To address this, we developed a new system (fig. S3) for generating a mosaic hindgut

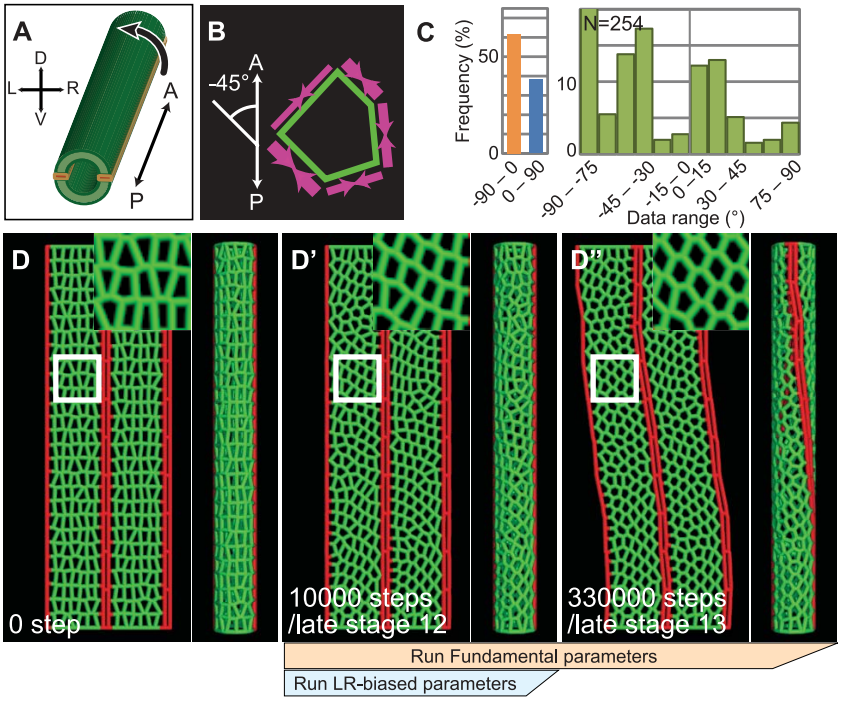

Fig. 4. Computer simulation suggesting that PCC may account for the left-handed rotation of the hindgut epithelial tube. (**A**) Diagram of the hindgut tube composed of epithelium (green) and two rows of boundary cells (orange). The direction of tube rotation is indicated by the curved arrow. (**B**) Diagram of the LR-biased constriction of cell boundaries (green). Arrows (magenta) show the constriction, whose magnitude corresponds to the width of the arrows (maximum at an angle $x°$ of −45°). (**C**) Percentage of modeled cell boundaries formed in silico with angle $x°$ of the ranges indicated at the bottom. (**D** to **D″**) Outputs of the simulation program. Green and red polygons are epithelial cells and boundary cells, respectively. Insets show higher-magnification images of framed areas. Steps in silico and the corresponding stages in vivo are indicated at the bottom of each panel.

epithelium composed of *Myo31DF*^{L152} homozygous cells with (+) or without (−) *Myo31DF*^{mEGFP} overexpression (Fig. 3E and fig. S3B). In the hindgut epithelium, the cell boundaries were classified into three types according to the cell type on either side (Fig. 3E): +/+, green; +/−, yellow; −/−, magenta. Cell boundaries of +/+ showed the wild-type LR bias of *D*E-Cad localization, which was reversed in the −/− boundaries (Fig. 3, F and H). The +/− cell boundaries did not show a statistically significant LR bias (Fig. 3G). Thus, the LR asymmetry of *D*E-Cad distribution at each cell boundary is attributable to the concordance of LR polarity in two adjacent cells.

To gain insight into how MyoID reverses the LR asymmetric distribution of *D*E-Cad, we looked for defects in endocytic trafficking, because *D*E-Cad's localization to the ZA is controlled by its recycling (*11*). Rab11-positive recycling endosomes became fewer in the apical-middle part of cells in *Myo31DF*^{L152} homozygotes compared with wild type, and this defect was restored by *Myo31DF*^{GFP} expression (fig. S4). These results may suggest that MyoID is involved in the recycling of *D*E-Cad.

Besides the angle $x°$, we also measured the length of cell boundaries at the ZA of the hindgut epithelial cells (fig. S5). In wild-type animals, the cell boundaries gradually expanded from late-stage 12 to late-stage 13 (fig. S5G). In homozygous *Myo31DF*^{L152} or *shg*^{R69} embryos, the length was greater than in wild type at all stages examined (fig. S5, B, E, and G). This increase was rescued by the overexpression of *Myo31DF*^{GFP} or *shg*^{DECH} in the respective mutant background (fig. S5, C, F, and G). Thus, *D*E-Cad and MyoID appear to restrict the expansion of these cell boundaries, suggesting that these proteins introduce cortical tension, possibly with LR asymmetry.

To evaluate our idea that PCC is involved in the hindgut LR asymmetric development, we built an in silico simulation model of the PCC of the hindgut epithelial cells and the directional rotation of the tube composed of these cells [see supporting online material (SOM) text for details] (figs. S6 to S9 and table S1). This model consisted of two epithelial sheets composed of model cells, forming the dorsal and ventral arcs of a tube with boundary cells separating the sheets, as found in vivo (Fig. 4A). In this simulation, the number of cells along the AP and LR sides was set to mimic the in vivo situation, and a statistical LR shape bias was not introduced initially (Fig. 4D). In vivo, *D*E-Cad was enriched at cell boundaries with an angle x of −90° to 0° and might restrict the cell-boundary expansion (Fig. 3, B and B′, and fig. S5G). Therefore, in this simulation, the constriction of cell boundaries was maximized at −45° to the AP axis of the hindgut epithelial tube, and the maximized value was twofold greater than at −135° or +45° (Fig. 4, B and D′). This parameter introduced PCC in the modeled epithelial cells (corresponding to late-stage 12) (Fig. 4, C and D′).

Because *D*E-Cad and MyoID were required before but not during the left-handed rotation of the hindgut epithelium, we did not add a LR bias to the cell-boundary constriction during the epithelial remodeling (simulation from the state of Fig. 4D′ to Fig. 4D″). The removal of LR bias subsequently led the modeled epithelial cells to assume stable cell shapes that were mostly regular hexagons (corresponding to late-stage 13) (Fig. 4D″). This progressive transition in cell shape was also observed in vivo (fig. S10). This simulation reproduced the 90° left-handed rotation of the epithelial tube in silico, suggesting that PCC is sufficient to explain this rotation in vivo (Fig. 4, D′ and D″, and movie S1). In addition, LR asymmetric changes in the cell-boundary length observed in the hindgut epithelium in vivo were recapitulated in the simulation, supporting the validity of our model (fig. S11).

We report PCC as a previously unknown mechanism of LR asymmetric morphogenesis. Various mutants of genes encoding the core components of planar cell polarity (PCP), a well-understood type of epithelial planar polarity, did not affect the laterality of the *Drosophila* embryonic gut (table S2), suggesting that PCC is not simply a variant of PCP. Although the importance of single-cell chirality has not been studied in multicellular organisms in vivo, intrinsic cell chirality has been found in the LR-polarized protrusion of neutrophil-like cells in vitro (*8*). Therefore, cell chirality may be a general property of animal cells. Our findings demonstrate a contribution of such chirality to LR asymmetric morphogenesis.

References and Notes

1. M. Levin, *Mech. Dev.* **122**, 3 (2005).
2. M. Hashimoto *et al.*, *Nat. Cell Biol.* **12**, 170 (2010).
3. C. Pohl, Z. Bao, *Dev. Cell* **19**, 402 (2010).
4. S. Hozumi *et al.*, *Nature* **440**, 798 (2006).
5. P. Spéder, G. Adám, S. Noselli, *Nature* **440**, 803 (2006).
6. J. A. Campos-Ortega, V. Hartenstein, *The Embryonic Development of* Drosophila melanogaster (Springer, Berlin, 1987).
7. F. C. de Anda *et al.*, *Nature* **436**, 704 (2005).
8. J. Xu *et al.*, *Proc. Natl. Acad. Sci. U.S.A.* **104**, 9296 (2007).
9. S. Etienne-Manneville, A. Hall, *Nature* **420**, 629 (2002).
10. U. Tepass *et al.*, *Genes Dev.* **10**, 672 (1996).
11. J. Langevin *et al.*, *Dev. Cell* **9**, 365 (2005).

Acknowledgments: We thank U. Tepass, S. Noselli, H. Oda, P. Adler, the Drosophila Genetic Resource Center at Kyoto Institute of Technology, and the Bloomington Drosophila Stock Center at Indiana University for flies and A. Nakamura and the Developmental Studies Hybridoma Bank for antibodies.

Supporting Online Material

www.sciencemag.org/cgi/content/full/333/6040/339/DC1
Materials and Methods
SOM Text
Figs. S1 to S11
Tables S1 and S2
References (*12*–*35*)
Movie S1

26 November 2010; accepted 10 June 2011
10.1126/science.1200940

Chirality in Planar Cell Shape Contributes to Left-Right Asymmetric Epithelial Morphogenesis

Kiichiro Taniguchi, Reo Maeda, Tadashi Ando, Takashi Okumura, Naotaka Nakazawa, Ryo Hatori, Mitsutoshi Nakamura, Shunya Hozumi, Hiroo Fujiwara, and Kenji Matsuno

Science **333** (6040), . DOI: 10.1126/science.1200940